CrystEngComm

Chemically Controlled Crystal Growth of $(CH_3NH_3)_2AgInBr_6$

Journal:	*CrystEngComm*
Manuscript ID	CE-COM-04-2018-000702.R1
Article Type:	Communication
Date Submitted by the Author:	25-May-2018
Complete List of Authors:	Tran, T.; Johns Hopkins University, Chemistry and Physics and Astronomy Quintero, Michael; Johns Hopkins University, Chemistry and Physics and Astronomy Arpino, Kathryn; Johns Hopkins University, Chemistry and Physics and Astronomy Kelly, Zachary; Johns Hopkins University, Chemistry and Physics and Astronomy Panella, Jessica; Johns Hopkins University, Chemistry Wang, Xiaoping; Oak Ridge National Laboratory, Chemical and Engineering Materials Division McQueen, Tyrel; Johns Hopkins University, Chemistry and Physics and Astronomy

SCHOLARONE™
Manuscripts

Please do not adjust margins

CrystEngComm

Communication

Chemically Controlled Crystal Growth of $(CH_3NH_3)_2AgInBr_6$

Thao T. Tran,[a] Michael A. Quintero,[a‡] Kathryn E. Arpino,[a§] Zachary A. Kelly,[a] Jessica R. Panella,[a] Xiaoping Wang*[b] and Tyrel M. McQueen*[ac]

Received 00th January 20xx,
Accepted 00th January 20xx

DOI: 10.1039/x0xx00000x

www.rsc.org/

We report the successful crystal growth of a previously unknown mixed-metal organic compound $(CH_3NH_3)_2AgInBr_6$. This phase, which is not obtained by direct combination of reactants, is crystallized through the use of Pb^{2+} (from $CH_3NH_3PbBr_3$) to modulate the soluble intermediates and force formation of $(CH_3NH_3)_2AgInBr_6$. Our results provide insights into mechanism and design-driven crystal growth and discovery of new halide materials that are chemically related to perovskites with photovoltaic and related applications.

Organic-inorganic methyl ammonium metal halides are of particular interest in the search for photoactive materials attributed to their rich structural and electronic behavior.[1-26] Their properties have been observed to be strongly correlated with the intricate interactions between the organic and inorganic subunits.[5,27-28] Structural dynamics within the perovskite structure h ave important implications for the operation mechanism of solar cells. They are thought to enhance charge carrier lifetime and open-circuit voltage, and affect hysteresis during current-voltage measurements.[29-31]

More specific to mixed metal-organic hybrids, it has been observed that organic-inorganic halide compounds, $(MA)_2MM'X_6$ (M = K, Tl, Ag; M' = Bi, Gd, Y; X = Cl, Br), are not as synthetically accessible as the inorganic derivatives ($Cs_2MM'X_6$ (M = Ag, M' = Bi, In, Sb; X = Cl, Br)).[2,8-11,32-36] That is due to the substantial difference between reactivity and decomposition and/or vaporization temperatures of the organic starting materials and those of the inorganic reagents, precluding high-temperature techniques and thus limiting synthetic options. $(MA)_2KBiCl_6$ and $(MA)_2TlBiBr_6$ have been synthesized by directly combining appropriate reagents hydrothermally.[2,8] The synthesis of $(MA)_2TlBiBr_6$, however, resulted in significant amounts of a by-product ($(MA)_3Bi_2Br_9$).[2] This issue was improved in the synthesis of $(MA)_2AgBiBr_6$ by adding $MAPbBr_3$, which was thought to serve as an *in situ* seed for the crystal growth.[9] This synthetic technique, however, did not selectively yield $(MA)_2AgBiBr_6$ and, as a secondary phase, $(MA)_3Bi_2Br_9$ was also formed.[9] Furthermore, the role of $MAPbBr_3$ in the synthesis has not been fully described and understood.

Here, we demonstrate synthesis strategy to rationally design a chemical reaction to create a product with desired structural units and/or physical properties. By implementing this strategy, we selectively synthesized and grew crystals of the new mixed metal halide $(MA)_2AgInBr_6$, which does not form as a major phase by a straightforward combination of starting materials, through the addition of $MAPbBr_3$. Rather than acting as an *in situ* seed, as has been previously postulated, we demonstrate that the key role is the formation of a complex intermediate species that selects a distinct reaction pathway. Thus, it offers a handle on how to design the synthesis of new hybrid halides.

In addition, this material undergoes a structural phase transition at T = 135 K, that is driven by the dynamic rotational disorder of MA units, i.e., the disordered MA groups pick one orientation over the others as temperature decreases, driving the structural packing of $(MA)_2AgInBr_6$ though hydrogen-bonding interactions (N-H---Br).

Initial synthetic attempts to prepare $(MA)_2AgInBr_6$ via direct combination or hydrothermal methods were unsuccessful due to decomposing and yielding AgBr and $(MA)_4InBr_7$. Yet, in one reaction, trace signs of a phase with composition $(MA)_2AgInBr_6$ was observed. To identify optimal synthesis conditions and gain better insight into the synthetic chemistry of $(MA)_2AgInBr_6$, a series of experiments were performed and they are summarized in Table S1.† The key observation is that the presence of $PbBr_2/MAPbBr_3$ is crucial for directing the selective formation of $(MA)_2AgInBr_6$. That the desired phase requires lead to form, despite it being a spectator species that is not in the final product, implies that it must be affecting the species in

a. Department of Chemistry, Department of Physics and Astronomy, Institute for Quantum Matter, Johns Hopkins University, Baltimore, MD 21218, United States
b. Neutron Scattering Division, Spallation Neutron Source, Oak Ridge National Laboratory, Oak Ridge, TN 39831, United States
c. Department of Materials Science and Engineering, Johns Hopkins University, Baltimore, MD 21218, United States

† Electronic Supplementary Information (ESI) available: Experimental methods, crystallographic tables, and additional data figures and analysis. See DOI: 10.1039/x0xx00000x

Please do not adjust margins

solution. For the reactions that do not involve lead, we find that three equilibrium reactions (1-3. Table S2)† provide a good approximation of the equilibria present during the synthesis of $(MA)_2AgInBr_6$ from a concentrated HBr solution.

For each reaction mentioned in Table S2,† there are an equilibrium constant K_{sp} and a reaction quotient Q. If the reaction condition could be altered in a way such that the reaction quotient $Q_1 \sim Q_3 >> Q_2$, $(MA)_2AgInBr_6$ would then crystallize. As the limiting reactants are $[Ag^+]$ and $[In^{3+}]$, $[MA^+]$ was changed to be either in excess or deficient to test whether the equilibria (1-3) were shifted to the favor of $(MA)_2AgInBr_6$ creation. As presented in Table S1,† the changes in the concentrations do not selectively yield the formation of $(MA)_2AgInBr_6$ as a major phase (Experiment (Exp) 1–6, Table S1).† Instead, the presence of lead in $MAPbBr_3$ is crucial for directing the synthetic reaction to form $(MA)_2AgInBr_6$ (Exp 7–9, Table S1).† $MAPbBr_3$ can be introduced to the synthesis either by providing $PbBr_2$ and MABr (Exp 7–8, Table S1)† or addition of *ex-situ* $MAPbBr_3$ crystals (Exp 9). Further, the fact that $(MA)_2AgInBr_6$ crystals were grown hydrothermally implies thermodynamic stability *under the conditions during growth*. It is not sufficient to add previously-prepared $(MA)_2AgInBr_6$ to act as a seed: growth of new material fails in the absence of $PbBr_2/MAPbBr_3$ (Exp 10, Fig. S1), with a significant fraction of the input crystalline $(MA)_2AgInBr_6$ decomposing into AgBr and $(MA)_4InBr_7$.† Together, our results imply that $PbBr_2/MAPbBr_3$, despite not being incorporated in the final product, guides the synthesis of $(MA)_2AgInBr_6$. The most likely mechanism is that the presence of Pb^{2+} modulates the formation of intermediates in solution, either by reducing the effective concentration of In^{3+} by binding, or increasing the solubility of AgBr (which is relatively insoluble, $K_{sp} = 5.4 * 10^{-14}$) and thus available concentration of Ag^{1+}, or some combination of the two.

To better understand the role of $PbBr_2/MAPbBr_3$ in the formation of $(MA)_2AgInBr_6$, we attempted to identify a hypothesized 'activated complex', which modulated intermediate during the reaction via UV-Vis spectroscopy (Fig. S2).† The UV-Vis spectra show that there are several equilibria present in the system, with transitions between discrete species (rather than shifts in absorption bands that would indicate formation of highly polymeric intermediates). Thus, to a good approximation, Jobs analysis can be used to identify the chemical compositions of the 'activated complex' $[(MA)_y(Ag_{1-x}Pb_x)]$, which is present as a dominant species in the system. We find that addition of lead significantly changes spectra in the presence of AgBr, and thus focus on potential intermediates containing Ag. The absorption maxima of $(MA)_4AgBr_5$, MABr and $MAPbBr_3$ solutions are observed at 245, 275 and 308 nm, respectively. With MABr in 100-fold excess, the ratio of Ag:Pb in $(Ag_{1-x}Pb_x)$ was determined to be 1:1 (x = 0.5) at the extrema (maximum or minimum) of the plots of the absorbance at a given wavelength as a function of the Pb composition (x) (Fig. 1) The amount of MA (y) in $[(MA)_y(AgPb)]$ was then identified to be 6 at the maxima of the plot (Fig. 1). This analysis resulted in the chemical composition of $[(MA)_6AgPb]Br_9$ of the 'activated complex'. The Lewis base strength of ligands likely present in the synthesis reactions can be arranged in order $CH_3NH_2 > Br^- > CH_3NH_3^+$. Under the acidic environment (concentrated HBr) of the synthesis, CH_3NH_2 (if present) is protonated, leaving Br- ligands most favourable to form chemical bonds to the central metal cations in the activated complex. For illustrative purposes, the symmetry arrangement of $[(MA)_6AgPb]Br_9$ consistent with the UV-Vis spectra is shown in Fig.1C.

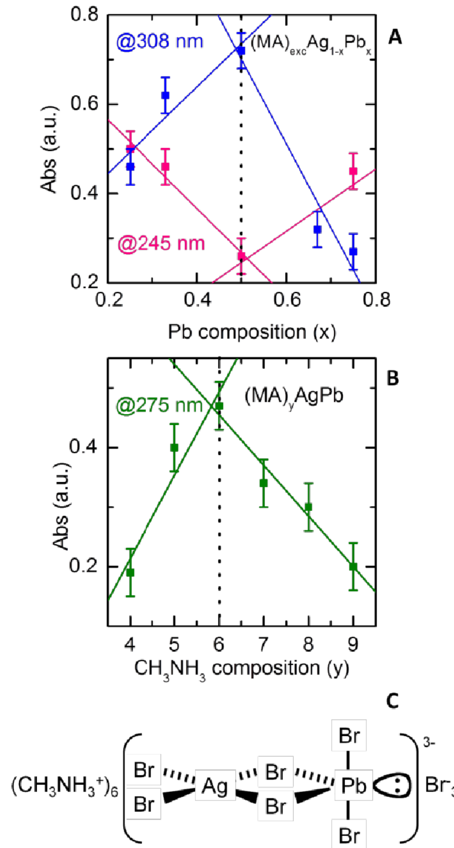

Fig. 1 Jobs analysis using UV-Vis spectroscopy (A-B). Absorbance at 308 nm and 245 nm (A) as a function of Pb composition (x) in $(MA)_{exc}Ag_{1-x}Pb_x$ with excess MABr; Absorbance at 275 nm (B) as a function of MA amount (y) in $(MA)_yAgPb$. The lines are fit to the data. (C) Proposed symmetry of the 'activated complex' with the chemical composition determined by Jobs analysis.

Thus, we find that, in the presence of $MAPbBr_3$, there are two additional equilibrium reactions (4-5, Table S2)† involved in the synthesis of $(MA)_2AgInBr_6$. $PbBr_2/MAPbBr_3$ shifts the equilibrium $(MA)_4AgBr_{5(aq)} + Pb^{2+}_{(aq)} + 2MA^+_{(aq)} + 4Br^-_{(aq)} \leftrightarrow [(MA)_6AgPb]Br_{9(aq)}$ ((4), Table S2)† to the formation of $[(MA)_6AgPb]Br_9$ 'activated complex'. $[(MA)_6AgPb]Br_9$, in turn, facilitates the $(MA)_2AgInBr_{6(s)}$ creation in $(MA)_2AgInBr_{6(s)} \leftrightarrow 2MA^+_{(aq)} + [Ag^+_{(aq)}]^* + In^{3+}_{(aq)} + 6Br^-_{(aq)}$ ((1), Table S2).† And $MAPbBr_3$ is also recovered with the formation of $(MA)_2AgInBr_6$. It is indicative of the Pb^{2+} cations in $MAPbBr_3$ playing two roles in this synthesis: (i) binding with free MA cations in solution, thus inhibiting the formation of $(MA)_4InBr_7$ by-product and (ii) interacting with the Ag^+ cations through the bridging Br in $[(MA)_6AgPb]Br_9$, thereby making Ag^+ available in solution. The

This journal is © The Royal Society of Chemistry 20xx

synthetic chemistry is illustrated in Fig. 2. Our results elucidate the vital roles of $MAPbBr_3$ in the synthesis, which does not simply serve as an *in situ* seed for crystal growth as thought previously[9].

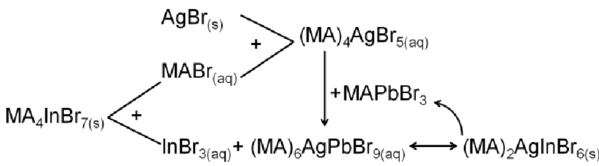

Fig. 2 Reaction scheme illustrating the synthetic chemistry of $(MA)_2AgInBr_6$

With single crystals of $(MA)_2AgInBr_6$ in hand, its crystal structures were fully characterized by single-crystal X-ray and neutron diffraction, as well as Rietveld powder XRD refinements (Fig. S3, Table S3-S5).†

Despite the apparent formula, $(MA)_2AgInBr_6$ ($A_2BB'X_6$) does not form with a double perovskite structure. This is attributed to a too large A/B cation ratio. Instead, $(MA)_2AgInBr_6$ crystallizes in the high symmetry trigonal space group $P\overline{3}m1$ (Fig. 3). The material exhibits a 1-dimensional chain of face-sharing alternating octahedra of $[AgBr_6]$ and $[InBr_6]$ and the MA cations are located in the empty space formed between the chains. This structure is similar to those of $BaNiO_3$ and $CsNiBr_3$,[37-38] which are composed of 1-dimensional chain of face-sharing $[NiO_6]$ and $[NiBr_6]$ octahedra, respectively. It is difficult to resolve the positions of light atoms, such as C, N and H, in the presence of the heavier Ag, In and Br atoms by X-ray diffraction alone. Neutron single-crystal diffraction was also used to resolve the structural orientation of the MA cations. The MA units are disordered about the the 2*d* sites, which are of C_{3v} point group symmetry. Each of the C and N atoms is assigned a partial occupancy of 1/6 accordingly. The hydrogen atoms were refined with rigid body RIGU restraints to account for the positional disorder and a rotational motion of the MA cations around the C–N axis. Similar disorder has also been observed in $MAPbI_3$.[39-40] Although $(MA)_2AgInBr_6$ and other known hybrid halides ($(MA)_2MBiX_6$ (M = K, Tl, Ag, X = Br, Cl) adopt the formula of double perovskite materials ($A_2BB'X_6$), the crystal structures of these hybrid materials are more diverse (from infinite 1-dimensional chain to 3-dimensional structures), compared to those of the other reported caesium mixed-metal halides $Cs_2BB'X_6$ (B = K, Tl, Ag, In B' = Sb, Bi, X = Br, Cl).[2,8-11,32-36] This may be due to the spatial anisotropy and dynamic disorder of the $CH_3NH_3^+$ units that have selective hydrogen-bonding interactions with the electronegative bromide atoms of the inorganic framework, thus driving the bonding patterns and structural features of the material at different temperatures.

To describe vibrations as well as confirm the C_{3v} symmetry of MA in the HT structure, IR study was performed (Fig. S4).† The vibrational modes observed in the IR spectra are consistent with those expected for the MA cation in C_{3v} symmetry (Γ_{vib} = 5A1 + A2 + 6E). The vibrational modes for $(MA)_2AgInBr_6$ were assigned and compared with $MAPbBr_3$.[41] The NH_3-related vibrational modes are stronger (in larger wavenumbers) than the corresponding CH_3 vibrations. That is attributed to the larger electronegativity of N compared to that of C, forming stronger N–H bonds, thereby enhancing the change in dipole moments associated with the NH_3 vibrations.

To determine optical bandgap for the material, the UV-Vis spectra were collected. The results indicate that $(MA)_2AgInBr_6$ exhibits bandgap with absorption edge value of 3.8 eV (Fig. S5).†

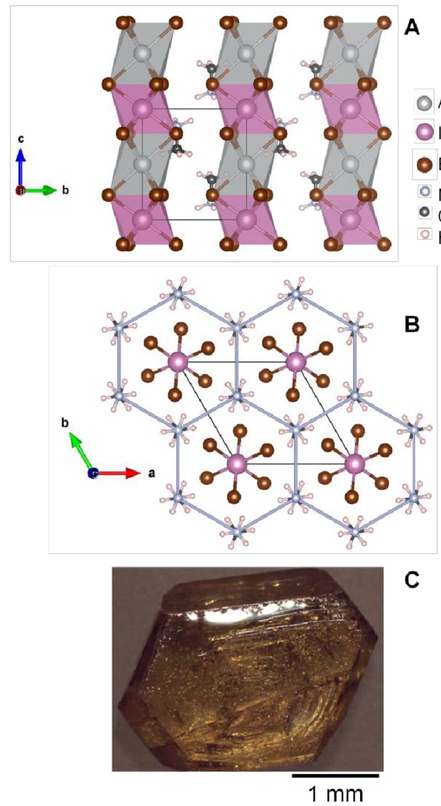

Fig. 3 Low-temperature (LT) crystal structure of $(CH_3NH_3)_2AgInBr_6$, (A) showing infinite 1-D chains of face-sharing $AgBr_6$ and $InBr_6$ octahedra and CH_3NH_3 (MA) units; (B) showing a 2-D buckled honeycomb-lattice of the MA units. High-temperature (HT) structure of $(MA)_2AgInBr_6$ is similar to LT structure, except the MA cations are disordered. (C)$(MA)_2AgInBr_6$ crystal

To investigate the thermal stability of $(MA)_2AgInBr_6$, thermogravimetric analysis (TGA) and differential scanning calorimetric (DSC) measurements were performed under Ar atmosphere. $(MA)_2AgInBr_6$ begins to melt at approximately 215 °C and partially decompose into $(MA)_4InBr_7$ and AgBr. Then further decomposition occurs at approximately 250 and 330 °C, corresponding to the loss of MABr and a mixture of MABr and $InBr_3$, respectively. The experimental weight loss is in excellent agreement with the calculated weight loss. The endothermic peaks in the heating curve are consistent with the melt and decomposition of $(MA)_2AgInBr_6$ (Fig. S6-S7).†

$(MA)_2AgInBr_6$ undergoes a structural phase transition at T = 135 K, observed in single crystal X-ray and neutron diffraction. The temperature-dependent structural analysis on single crystals is challenging as crystals tend to develop multiple domains (twinning) due to mechanical strain occurred with changing temperature. In the low temperature (LT) data, the crystal was found to be a four-domain twin. By incorporating the correct twin law, the least-squares refinements were significantly improved and converged. The LT structure crystallizes in the low symmetry trigonal space group $P\overline{3}$. The nature of the structural transition is driven by the dynamic disorder of the MA units, i.e., the disordered MA cations pick one orientation over the others at low temperature, directing the structural change through the hydrogen-bonding interactions (N – H- - -Br) (Fig. 4). The MA units in both structures are patterned on a 2-D buckled honeycomb lattice, illustrating an example of proton ordering in two dimensions (Fig. 3). The order of protons occurring simultaneously at six sites, rather than just adjacent sites, gives rise to the directional movement of the Br atoms in the LT structure compared to those in the HT structure while the positions of Ag and In stay essentially unchanged.

The presence of hydrogen atoms in the structures was located from negative nuclear scattering density. In HT structure, due to dynamic disorder of the MA cation, six possible – NH_3^+ positions of MA cation generate N–H---Br bonding interactions with H---Br distances range from 2.75(5) to 2.81(7) Å. In LT structure, the hydrogen bonding distances reduce to 2.760(3) and 2.805(4) Å. Hydrogen bonding interactions are depicted in Fig. 4 (and Table S4-S5).†

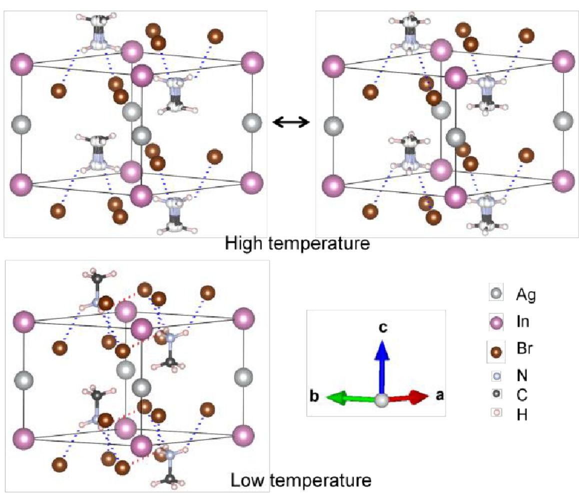

Fig. 4 Hydrogen bond interactions in high temperature (HT) (two major microstates) and low temperature (LT) structure of $(CH_3NH_3)_2AgInBr_6$. Hydrogen-bond geometry (*D*(donor)—H···*A*(acceptor)) for N1—H1···Br1 at LT from neutron diffraction: *D*—H 1.011(3) Å; H···A 2.760(3) Å, 2.805(3) Å; D···A 3.5142(9) Å, 3.6468(5) Å; D—H···A 131.7(3)°, 141.0(2).

In addition to the structural analysis, the nature of the phase transition was studied by the specific heat measurements. In a plot of C_p vs. T, Fig. 5, there is a peak indicative of the structural phase transition at T = 135 K and no hysteresis is observed from the heating and cooling curves (Fig. S8).† In addition, there is group-subgroup relationship between the HT and LT crystal structures ($P\overline{3}m1 \leftrightarrow P\overline{3}$). Thus, this is likely a second-order phase transition. In addition, the changes in entropy were estimated from a plot of C_p/T vs. T to be ΔS = 5.79 J mol f.u.$^{-1}$ K^{-1} ≈ Rln2 after subtracting phonon contribution, which was approximated from a coefficient/T (Fig. 5). This is roughly half the value expected for one degree of freedom (two microstates) per methylammonium unit, implying significant correlations in MA^+ cation motion above the phase transition. This is not unexpected, as the one dimension columns of Ag/$InBr_6$ octahedra enforce a coupling between adjacent MA^+ ions (through the hydrogen bonding interactions).

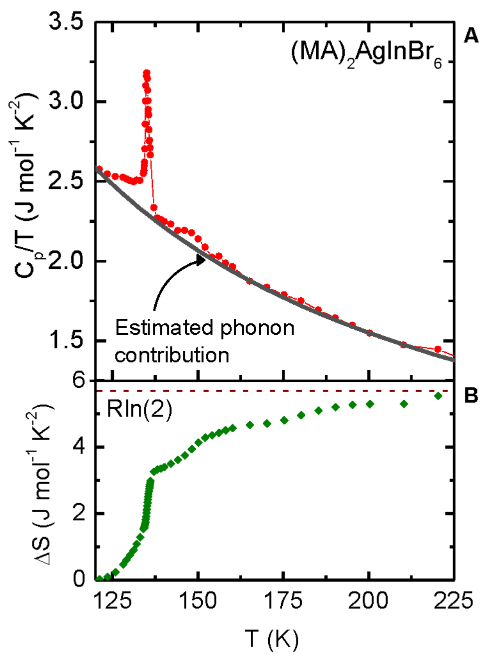

Fig. 5 (A) Heat capacity (C_p/T) of $(CH_3NH_3)_2AgInBr_6$ as a function of temperature, showing a structural phase transition at 135 K; (B) the changes in entropy estimated from the integration of the peak after subtracting phonon contribution.

Conclusions

In short, we have found that $PbBr_2$/$MAPbBr_3$ can be used to induce the formation of new organic-inorganic hybrid materials. The key mechanism is not acting as a seed for preferential crystal growth, but rather affecting the equilibrium distribution of species in solution, allowing for selective control of the thermodynamically stable phase (Fig. 2). Further, we find that the spatial anisotropy and dynamics of the MA units gives rise to the sensitivity of crystal structures and thus properties to temperature. That paves an avenue to discover unconventional physical phenomena of hybrid materials containing organic components with dynamic motions. Our results provide insights into the mechanisms and design-driven synthesis and discovery for new organic-inorganic halide materials that are chemically related to perovskites with photovoltaic and related applications.

This journal is © The Royal Society of Chemistry 20xx

Conflicts of interest

There are no conflicts to declare.

Acknowledgements

Support from the Johns Hopkins University, Krieger School of Art and Sciences, Faculty Innovation Award is gratefully acknowledged. UV-Vis data were collected using instrumentation acquired under the NSF, Division of Materials Re-search (DMR), Solid State Chemistry (SSMC) CAREER grant under Award DMR-1253562. TMM acknowledges support from the David and Lucile Packard Foundation and the Sloan Research Fellowship. Single crystal neutron diffraction used resources at the Spallation Neutron Source, a DOE Office of Science User Facility operated by the Oak Ridge National Laboratory, under Contract No. DE-AC05-00OR22725 with UT-Battelle, LLC. We thank Prof. Thomas Kempa, Alexander Kossak and Ben Stephens for TEM experiments. We thank W. A. Phelan for assistance with the TGA/DSC measurements, carried out at the PARADIM Bulk Materials Facility, as part of the Materials for Innovation Platform Program, which is supported by the National Science Foundation (Grant DMR-1539918).

Present address

‡Department of Chemistry, Northwestern University, Evanston, Illinois 60208, United States
§Max Planck Institute for Chemical Physics of Solids, Dresden 01187, Germany

References

1 Li, W.; Wang, Z.; Deschler, F.; Gao, S.; Friend, R. H.; Cheetham, A. K. *Nat. Rev. Mater.* 2017, **2**, 16099.
2 Deng, Z.; Wei, F.; Sun, S.; Kieslich, G.; Cheetham, A. K.; Bristowe, P. D. *J. Mater. Chem. A* 2016, **4**, 12025-12029.
3 Fabini, D. H.; Hogan, T.; Evans, H. A.; Stoumpos, C. C.; Kanatzidis, M. G.; Seshadri, R. *J. Phys. Chem. Lett.* 2016, **7**, 376-381.
4 Hao, F.; Stoumpos, C. C.; Cao, D. H.; Chang, R. P. H.; Kanatzidis, M. G. *Nat. Photonics* 2014, **8**, 489-494.
5 Hutter, E. M.; Gelvez-Rueda, M. C.; Osherov, A.; Bulovic, V.; Grozema, F. C.; Stranks, S. D.; Savenije, T. J. *Nat. Mater.* 2017, **16**, 115-120.
6 Mao, L.; Wu, Y.; Stoumpos, C. C.; Wasielewski, M. R.; Kanatzidis, M. G. *J. Am. Chem. Soc.* 2017, **139**, 5210-5215.
7 Tsai, H.; Nie, W.; Blancon, J.-C.; Stoumpos, C. C.; Asadpour, R.; Harutyunyan, B.; Neukirch, A. J.; Verduzco, R.; Crochet, J. J.; Tretiak, S.; Pedesseau, L.; Even, J.; Alam, M. A.; Gupta, G.; Lou, J.; Ajayan, P. M.; Bedzyk, M. J.; Kanatzidis, M. G.; Mohite, A. D. *Nature* 2016, **536**, 312-316.
8 Wei, F.; Deng, Z.; Sun, S.; Xie, F.; Kieslich, G.; Evans, D. M.; Carpenter, M. A.; Bristowe, P. D.; Cheetham, A. K. *Mater. Horiz.* 2016, **3**, 328-332.
9 Wei, F.; Deng, Z.; Sun, S.; Zhang, F.; Evans, D. M.; Kieslich, G.; Tominaka, S.; Carpenter, M. A.; Zhang, J.; Bristowe, P. D.; Cheetham, A. K. *Chem. Mater.* 2017, **29**, 1089-1094.
10 Yokoyama, T.; Song, T.-B.; Cao, D. H.; Stoumpos, C. C.; Aramaki, S.; Kanatzidis, M. G. *ACS Energy Lett.* 2017, **2**, 22-28.
11 Deng, Z.; Wei, F.; Brivio, F.; Wu, Y.; Sun, S.; Bristowe, P. D.; Cheetham, A. K. *J. Phys. Chem. Lett.* 2017, **8**, 5015-5020.
12 Bennett, T. D.; Cheetham, A. K.; Fuchs, A. H.; Coudert, F.-X. *Nat. Chem.* 2016, **9**, 11-16.
13 Ke, W.; Stoumpos, C. C.; Spanopoulos, I.; Mao, L.; Chen, M.; Wasielewski, M. R.; Kanatzidis, M. G. *J. Am. Chem. Soc.* 2017, **139**, 14800-14806.
14 Cao, D. H.; Stoumpos, C. C.; Yokoyama, T.; Logsdon, J. L.; Song, T.-B.; Farha, O. K.; Wasielewski, M. R.; Hupp, J. T.; Kanatzidis, M. G. *ACS Energy Lett.* 2017, **2**, 982-990.
15 Hartmann, C.; Sadoughi, G.; Félix, R.; Handick, E.; Klemm, H. W.; Peschel, G.; Madej, E.; Fuhrich, A. B.; Liao, X.; Raoux, S.; Abou-Ras, D.; Wargulski, D.; Schmidt, T.; Wilks, R. G.; Snaith, H.; Bär, M. *Adv. Mater. Interfaces* 2018, **1701420**, 1-9.
16 Guzelturk, B.; Belisle, R. A.; Smith, M. D.; Bruening, K.; Prasanna, R.; Yuan, Y.; Gopalan, V.; Tassone, C. J.; Karunadasa, H. I.; McGehee, M. D.; Lindenberg, A. M. *Adv. Mater.* 2018, **1704737**, 1-8.
17 Fabini, D. H.; Siaw, T. A.; Stoumpos, C. C.; Laurita, G.; Olds, D.; Page, K.; Hu, J. G.; Kanatzidis, M. G.; Han, S.; Seshadri, R. *J. Am. Chem. Soc.* 2017, **139**, 16875-16884.
18 Laurita, G.; Fabini, D. H.; Stoumpos, C. C.; Kanatzidis, M. G.; Seshadri, R. *Chemical Science* 2017, **8**, 5628-5635.
19 Li, L.; Sun, Z.; Wang, P.; Hu, W.; Wang, S.; Ji, C.; Hong, M.; Luo, J. *Angew. Chem., Int. Ed.* 2017, **56**, 12150-12154.
20 (20) Schelhas, L. T.; Christians, J. A.; Berry, J. J.; Toney, M. F.; Tassone, C. J.; Luther, J. M.; Stone, K. H. *ACS Energy Lett.* 2016, **1**, 1007-1012.
21 Kubicki, D.; Prochowicz, D.; Hofstetter, A.; Saski, M.; Yadav, P.; Bi, D.; Pellet, N.; Lewinski, J.; Zakeeruddin, S. M.; Gratzel, M.; Emsley, L. *J Am Chem Soc* 2018, **DOI: 10.1021/jacs.7b12860**.
22 Ummadisingu, A.; Gratzel, M. *Sci. Adv.* 2018, **4**, e1701402.
23 Dualeh, A.; Gao, P.; Seok, S. I.; Nazeeruddin, M. K.; Gratzel, M. *Chem. Mater.* 2014, **26**, 6160-6164.
24 Bag, M.; Renna, L. A.; Adhikari, R. Y.; Karak, S.; Liu, F.; Lahti, P. M.; Russell, T. P.; Tuominen, M. T.; Venkataraman, D. *J. Am. Chem. Soc.* 2015, **137**, 13130-13137.
25 Huang, W.; Manser, J. S.; Kamat, P. V.; Ptasinska, S. *Chem. Mater.* 2016, **28**, 303-311.
26 Aristidou, N.; Sanchez-Molina, I.; Chotchuangchutchaval, T.; Brown, M.; Martinez, L.; Rath, T.; Haque, S. A. *Angew. Chem., Int. Ed.* 2015, **54**, 8208-8212.
27 Frost, J. M.; Butler, K. T.; Brivio, F.; Hendon, C. H.; van Schilfgaarde, M.; Walsh, A. *Nano Lett.* 2014, **14**, 2584-2590.
28 Brivio, F.; Butler, K. T.; Walsh, A.; van Schilfgaarde, M. *Phys. Rev. B: Condens. Matter Mater. Phys.* 2014, **89**, 155204/155201-155204/155206.
29 Leguy, A. M. A.; Azarhoosh, P.; Alonso, M. I.; Campoy-Quiles, M.; Weber, O. J.; Yao, J.; Bryant, D.; Weller, M. T.; Nelson, J.; Walsh, A.; van Schilfgaarde, M.; Barnes, P. R. F. *Nanoscale* 2016, **8**, 6317-6327.

This journal is © The Royal Society of Chemistry 20xx

30 Quarti, C.; Mosconi, E.; De Angelis, F. *Chem. Mater.* 2014, **26**, 6557-6569.
31 Wu, B.; Fu, K.; Yantara, N.; Xing, G.; Sun, S.; Sum, T. C.; Mathews, N. *Adv. Energy Mater.* 2015, **5**, 1500829.
32 McClure, E. T.; Ball, M. R.; Windl, W.; Woodward, P. M. *Chem. Mater.* 2016, **28**, 1348-1354.
33 Slavney, A. H.; Hu, T.; Lindenberg, A. M.; Karunadasa, H. I. *J. Am. Chem. Soc.* 2016, **138**, 2138-2141.
34 Volonakis, G.; Haghighirad, A. A.; Milot, R. L.; Sio, W. H.; Filip, M. R.; Wenger, B.; Johnston, M. B.; Herz, L. M.; Snaith, H. J.; Giustino, F. *J. Phys. Chem. Lett.* 2017, **8**, 772-778.
35 Filip, M. R.; Hillman, S.; Haghighirad, A. A.; Snaith, H. J.; Giustino, F. *J. Phys. Chem. Lett.* 2016, **7**, 2579-2585.
36 Tran, T. T.; Panella, J. R.; Chamorro, J. R.; Morey, J. R.; McQueen, T. M. *Mater. Horiz.* 2017, **4**, 688-693.
37 Takeda, Y.; Kanamaru, F.; Shimada, M.; Koizumi, M. *Acta Cryst. B* 1976, **32**, 2464-2466.
38 Raw, A. D.; Ibers, J. A.; Poeppelmeier, K. R. *J. Solid State Chem.* 2012, **192**, 34-37.
39 Weller, M. T.; Weber, O. J.; Henry, P. F.; Di Pumpo, A. M.; Hansen, T. C. *Chem. Commun.* 2015, **51**, 4180-4183.
40 Ren, Y.; Oswald, I. W. H.; Wang, X.; McCandless, G. T.; Chan, J. Y. *Cryst. Growth Des.* 2016, **16**, 2945-2951.
41 Cabana, A.; Sandorfy, C. *Spectrochim. Acta* 1962, **18**, 843-861.

This journal is © The Royal Society of Chemistry 20xx